10.1149/06427.0021ecst

Development of Representative Tests to Quantify the Susceptibility to Stress Corrosion Cracking of α,β'-Brass Used for Gas Transfer Devices

C. Berne[a, b, c], E. Andrieu[b], J. Reby[c], J-M. Sobrino[d], and C. Blanc[b]

[a] PhD candidate, joint laboratory CETIMAT, CETIM – CIRIMAT
[b] Université de Toulouse, CIRIMAT, UPS / INPT / CNRS, Equipe MEMO
ENSIACET, 4, allée Emile Monso BP 44362, 31030 Toulouse Cedex 4, France
[c] CETIM, Pôle Matériaux Métalliques et Surface
74, route de la Jonelière CS 82617, 44326 Nantes Cedex 3, France
[d] CETIM, Pôle Matériaux Métalliques et Surface
52, Avenue Félix Louat CS 80067, 60304 Senlis Cedex, France

Corrosion susceptibility of an α,β'-brass CuZn40Pb2 (CW617N), used for gas transfer devices, was investigated through accelerated corrosion tests at a constant anodic potential in $NaNO_3$ solution with basic pHs. The anodic dissolution behavior of the α,β'-brass was characterized by a two stages-mechanism, with each stage including both dezincification and simultaneous dissolution phenomena of the β' phase but with different kinetics at each stage. Compressive or tensile stresses applied on brass specimens during the accelerated tests were observed largely to influence the anodic dissolution kinetics. Stresses were assumed to open or close the pores present in the dezincified β' phase, which promoted or slowed the dezincification mechanism, including with the Zn diffusion into the solution trapped inside of the pores.

Introduction

Gaz transfer valves composed of α,β'-brasses and used in a various range of environmental conditions were analyzed after failure generated in service. Through-cracking phenomena were observed attributed to SCC damage coupled with simultaneous dissolution (Cu, Zn) and/or selective dissolution (Zn, dezincification) processes. Dissolution phenomena are expected to play a major role during the first stages (incubation and initiation) of stress corrosion cracking (SCC) damage, leading to rupture, that can be observed on the network components in service. Failure analyses of some components showed a strong dissolution phenomenon through all the depth of the material, and a dissolution assisted by the stress until the rupture was expected. On balance, the dissolution phenomena were identified as the elementary corrosion mechanism to study in order to develop representative accelerated tests to evaluate the susceptibility to corrosion and SCC of α,β'-brasses and to ensure a long term durability of brass components.

In literature, the corrosion behavior of α-brass was largely studied (in nitrite solutions, for example: (1) (2) (3) (4) (5) (6) (7) (8) (9) (10)) but not the corrosion behavior of α,β'-brasses (11) (12) (13) (14). The dissolution mechanisms proposed in the literature for metallic alloys (15) are divided into two categories: selective and non-selective. The non-selective mechanism refers to a complete dissolution of metallurgical phases of the alloys.

Regarding brasses, selective mechanisms correspond to dezincification, and here two main mechanisms have also been distinguished. The first corresponds to a preferential dissolution of Zn controlled by Zn diffusion in the Cu-rich phase that has been formed. The second corresponds to a simultaneous dissolution of Zn and Cu, which turns into a preferential dissolution with re-deposition of Cu in solution (16). The present study aimed to contribute to a better understanding of the dissolution processes of α,β'-brass under a constant anodic potential in a $NaNO_3$ solution in the framework of the development of accelerated SCC tests. The approach consisted in testing the influence of the environment (pH, potential) and mechanical stress on the dissolution kinetics. In the present work, α,β'-brass CuZn40Pb2 (CW617N) was studied; samples were removed from stamping rods that were used to manufacture gas transfer valves. CW617N is used principally for its good machinability and resistance to corrosion, and particularly for water taps manufacture (17) (18) (19) (20). $NaNO_3$ solutions were selected to perform accelerated corrosion tests on the basis of preliminary results and a literature review on α-brass (21) although the solutions that are most often used are ammonia (14) (22) (23), sulfuric acid (15) (24) (25), and nitrite solutions (9). The discussion section focuses on the identification of dissolution mechanisms and key parameters controlling the dissolution kinetics. The influence of compressive or tensile stresses on the dissolution mechanisms was discussed to understand the SCC incubation and initiation stages (i.e., crack initiations) better.

Experimental

Material

The heart of a 65mm diameter stamping rod of the α,β'-brass CuZn40Pb2 (CW617N; Zn 38.35, Al 0.008, Ni 0.051, Fe 0.205, Mn 0.004, Sn 0.150, Pb 1.875, Si 0.001, Cu 59.35, wt. %) was used to sample the material studied in the present work. The α phase (64 at% Cu, 36 at% Zn) was included in an enveloping β' phase (55at% Cu, 45at% Zn), which is in agreement with the solidification processes expected for CuZn40Pb2 alloys (Figure 1). Equiaxed grains (α and β' phase) with an average size of 24 µm in diameter for the α phase and 20µm for the β' phase were observed in the transverse section of the rod, whereas, in the longitudinal sections of the rod, a texturation of the β' grains (their size varied from 20µm to 120µm in the longitudinal direction compared to 20µm in the transverse direction) was detected. Moreover, a preferential germination of α grains at the β' grain boundaries led to an heterogenous distribution of α and β' in this section of the material.

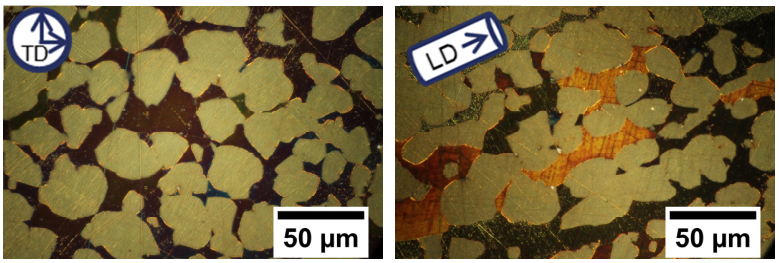

Figure 1. Optical microscope observations of the α,β'-brass CuZn40Pb2 (CW617N)

Corrosion tests

A 0.5M $NaNO_3$ solution (AnalaR NORMAPUR® ACS, ISO, Reag. Ph. Eur. analytical reagent) with adjusted pH (11 or 12) by the addition of NaOH (AnalaR NORMAPUR® ACS, ISO, Reag. Ph. Eur. analytical reagent) was prepared for all corrosion tests. A first set of corrosion tests at constant anodic potential (20 mV/SCE or 50 mV/SCE) without mechanical stress was performed with a standard device composed of a potentiostat connected to a reference electrode (Saturated Calomel Electrode), a counter electrode (platinum) and a working electrode composed of an α,β'-brass sample. The surface exposed to the electrolyte corresponded to the plane perpendicular to the extrusion direction. In reference conditions, a surface area of 0.2 cm^2 (ratio surface/volume = 6.7. 10^{-4} cm^2/mL) was selected by using a varnish. The sample surface was polished with 4000 grit SiC paper before the experiment. Tests were performed in a beaker with 300 mL of the solution that was open to the air and that was moderately stirred with a magnetic stirrer. During the tests, the beakers were placed in a thermostatically controlled water-bath maintained at 23.5±2 °C.

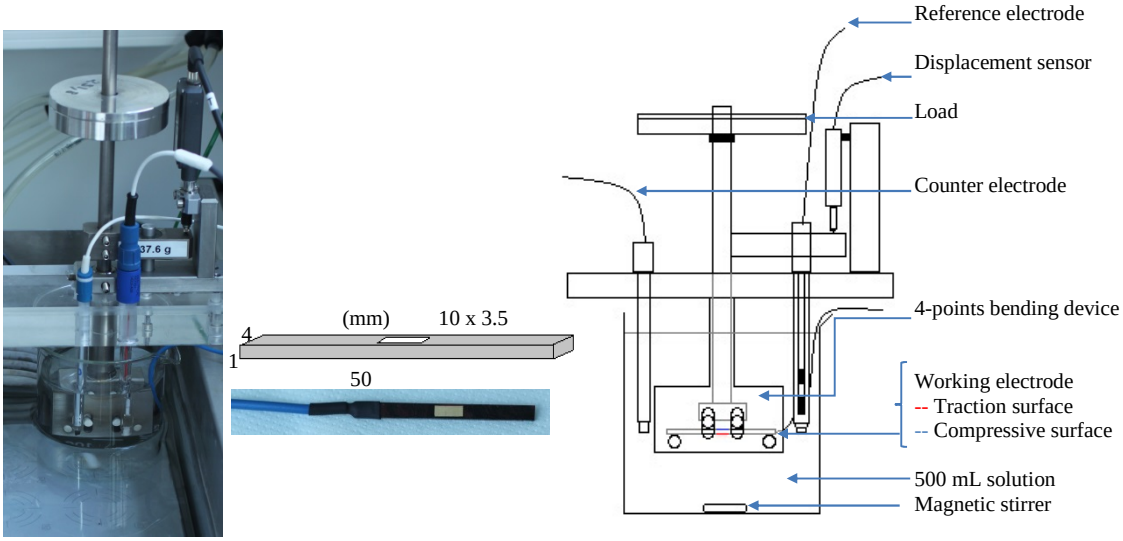

Figure 2. Bending device used to determine the influence of a mechanical stress on the open circuit potential values, anodic polarization curves, and corrosion test results at a constant potential and geometry of the specimen.

A second set of experiments was performed to study the influence of a mechanical stress on the corrosion behavior of the α,β'-brass CuZn40Pb2 using a bending device developed in the laboratory (Figure 2), allowing for the specimen to be completely immersed in 500 mL of the electrolyte solution. Geometry of the tested specimen is also presented in Figure 2. The stress was perpendicular to the extrusion direction. Either surface under tensile or compressive stress was exposed to the electrolyte using a protective varnish on the non-exposed surface. In each case, the surface exposed to the electrolyte corresponded to a zone in a rectangular shape (10 x 3.5 mm^2; ratio surface/volume = 7. 10^{-4} cm^2/mL) in the center of the specimen between the two interior support rollers. An initial maximal stress of 140 MPa was applied to achieve 70% of the yield strength at 0.2% of strain, which was previously determined by traction tests at $10^{-3}s^{-1}$ and found to be 205 MPa. The corrosion tests were then performed at constant mechanical stress. Displacements during the tests were followed with a sensor (Keyence-GT2-H12K). During the tests, the potential was applied using the same standard device

used for the corrosion tests without mechanical stress (Potentiostat, 3 electrodes with the brass as the working electrode, magnetic stirring, and thermostatically controlled water-bath).

For corrosion tests with or without mechanical stress, the potential was applied after 15 minutes of immersion at the open circuit potential (OCP). The duration of the corrosion tests was between 2 and 48h.

Complementary tests

Cross-sections of the corroded material were prepared after corrosion tests at constant potential to follow the corrosion propagation. They were observed using an optical microscope (OM, NIKON) to measure the dissolution depths. More detailed observations were also performed by using a scanning electron microscope (SEM, LEO 435VP) coupled with an Energy-dispersive X-ray spectrometer (EDS) for chemical analyses. The evolution of the corrosive solution was followed by a pH-meter and X-ray diffraction (XRD) experiments were performed on solid corrosion products removed and dried from the solution after corrosion tests: 2-θ scans were performed from 20° to 70° using Cu K-α radiation and SEIFERT-3000TT equipment.

Results

Figure 3 presents the typical damage caused by the corrosion tests at a constant potential in the conditions called reference conditions (0.5M $NaNO_3$ solution, at pH 11, without mechanical stress and under 50mV/SCE; surface/volume ratio equal to a 0.2cm² surface per 300 mL of solution).

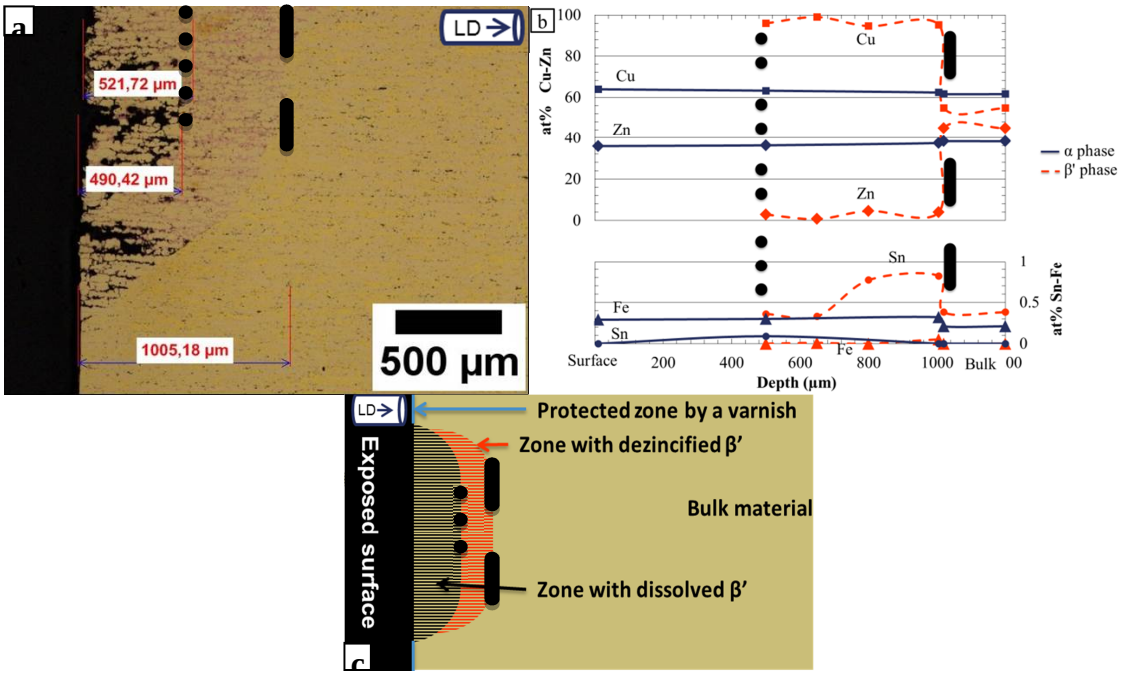

Figure 3. Analysis of a cross-section of the α,β'-brass CuZn40Pb2 sample after a 48h corrosion test at the reference set, i.e., 0.5 M $NaNO_3$ solution at pH 11 under anodic polarization at 50 mV/SCE by (a) optical microscope and (b) EDX analysis. (c) Scheme of the corrosion damage.

The damage area evidenced an elliptical shape corresponding to the β' phase dissolution. The dissolution starts at the edges of the exposed zone that was separated from the protected zone by a varnish (scheme in Figure 3 c). Due to the shape of the damage area (dissolution depth constant in the center of the exposed area), the quantification of the corrosion damage, i.e., dissolution measurements, was performed in the center of the corroded zone. Two types of dissolution were identified. The first type was a complete dissolution of the β' phase, corresponding essentially to a simultaneous dissolution of Cu and Zn present in this phase. β' complete dissolution led to a porous layer composed of non-corroded α grains only. The second type of dissolution was a selective dissolution of Zn contained in the β', called dezincification. This second process was easily identified by OM with discoloring of the β' phase which became pink-colored but remained around the non-corroded α phase. Chemical analyses by EDX were performed through the sections of the corroded specimens (Figure 3 b). The discolored β' phase was identified as a Cu-rich phase, totally depleted in Zn. No gradient of the Zn content was observed through the thickness of the dezincified layer. To quantify the dissolution damage, two parameters were identified and recorded versus the duration of the corrosion tests: the depth of the simultaneous dissolution front, i.e., the average distance between the initial surface of the material and the first β' grain not completely dissolved, and the depth of the dezincification front, i.e., the average distance between the initial surface of the material and the first intact β' grain. This method was chosen to evaluate the kinetics of dissolution because the depth of dissolution is expected to be one of the decisive factors for the lifetime of brass component. Figure 4 shows the dissolution depth vs. time curves: each point corresponds to an independent corrosion test at a constant potential where both dissolution depths were measured. The results for the reference conditions were characterized by a two stages-mechanism separated by a critical time equal to 18 hours:

- In the first stage (t< 18h) the dezincification front merged with the simultaneous dissolution front. OM observations in the cross-sections showed the presence of a porous structure that consisted of a non-corroded α phase only on the outer layer of the sample but possessed no discoloring of the β' phase, i.e., no visible signs of a Cu-rich phase, under this outer layer.
- In the second stage (t> 18h) the dezincification front preceded the dissolution front. At this stage, the porous structure corresponding to the simultaneous dissolution of the β' phase was still observed in the outer layer but an inner layer was observed. This inner layer was composed of non-corroded α grains and a porous copper-rich phase replacing the β' phase, which was pink-colored. These observations clearly show that, during the second stage, the complete dissolution of the β' phase was not stopped but continued to proceed with a time lag compared to the dezincification.

Effects of potential and pH. To identify the effect of the two parameters on the dissolution kinetics, the results obtained with different experimental conditions were compared with those obtained for the reference conditions. The results are presented in Figure 4.

- At a lower potential than that of the reference conditions, i.e., 20 mV/SCE (Figure 4 a), results showed a first stage where both dissolution depths were very low. After a critical time, a significant evolution of the simultaneous dissolution front and the dezincification front was observed. From this time, the kinetics of the dezincification process became very quickly higher than that of the simultaneous dissolution. Then both

kinetics of dissolution were lower than those for a 50 mV/SCE potential but the global shape of depth vs time curves were similar to that of the higher potential.
- At higher pH than that of the reference condition, i.e. pH 12, results showed also a first stage where the kinetics of both dissolution processes were similar but were more critical for pH 11 than pH 12. In the first few hours, the kinetics of dissolution were very low at pH 12. After a critical time equal for both pHs, the second stage initiated with the dezincification front preceding the dissolution front; during this stage, the kinetics of both dissolution processes became higher at pH 12 compared to pH 11.

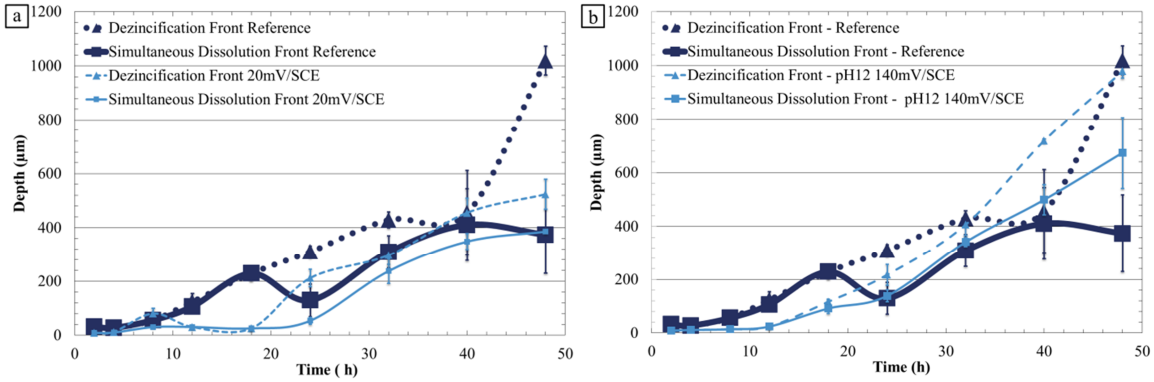

Figure 4. Influence of (a) applied potential and (b) pH on the dissolution depths (i.e., simultaneous dissolution and dezincification) of the α,β' brass CuZn40Pb2. In each graph, the effect of the specific parameter is studied in comparison with the results obtained for the reference conditions, i.e., experiments in a 0.5 M $NaNO_3$ solution, a pH adjusted to 11, and an applied potential equal to 50 mV/SCE.

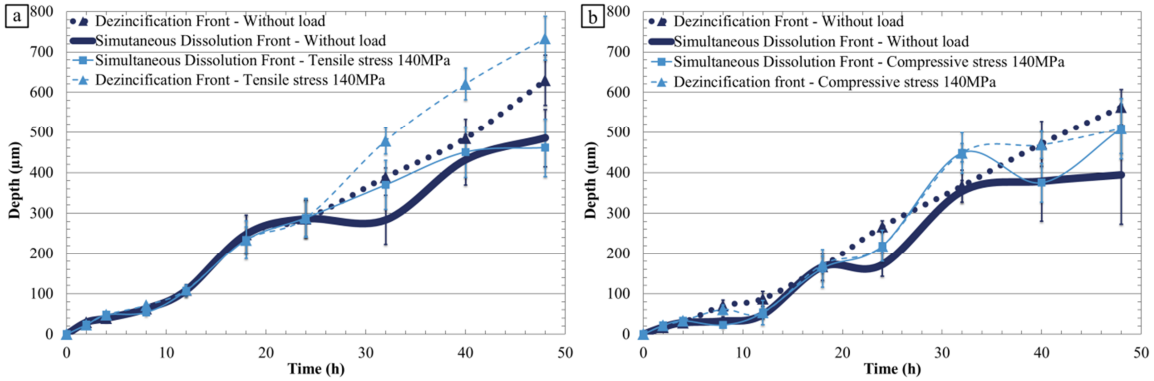

Figure 5. Influence of (a) tensile mechanical stress and (b) compressive mechanical stress on the depth of the dissolution (i.e., complete dissolution and dezincification) of the α,β' brass CuZn40Pb2. In each graph, the effect of the mechanical stress is studied in comparison with the results obtained for the reference conditions, i.e., experiments in a 0.5 M $NaNO_3$ solution, a pH adjusted to 11, and an applied potential equal to 50 mV/SCE without mechanical stress.

Effect of a mechanical stress. Figure 5 shows the effects of a mechanical stress on the dissolution kinetics, i.e., simultaneous dissolution and dezincification. New curves of dissolution depths vs time for the reference conditions were plotted with samples placed on the bending device without applying a mechanical stress to eliminate the effects of the bending device (stirring, position of the exposed surface) and to have the same surface/volume ratio with and without a mechanical stress. This explained the differences

in the reference curves in comparison to those plotted in Figure 4. Comparison of the curves plotted in Figure 5, without stress and with stress, allowed to identify the isolated effect of a compressive or tensile stress. As previously described, all curves evidenced two stages with a first stage corresponding to similar kinetics for both simultaneous dissolution and dezincification and, after a critical time, a second stage where dezincification occurred faster than the simultaneous dissolution. Concerning the effect of mechanical stress, major results were that:

(i) there was no effect of a tensile mechanical stress on the first stage and on the critical time compared to samples without a mechanical stress. However, under tensile mechanical stress, the dezincification kinetics were significantly affected during the second stage. Dezincification process under tensile stress was faster than in the reference conditions without mechanical stress while the simultaneous dissolution process was not significantly affected during the entire corrosion test (Figure 5 a)

(ii) under compressive mechanical stress, the simultaneous dissolution and dezincification processes were similar over long periods of time compared to the results without mechanical stress (Figure 5 b). The depths of dezincification were never significantly deeper than the depths of complete dissolution.

Previous results evidenced that stirring significantly influenced the results. Indeed, dissolution kinetics for the reference conditions where quite affected by the use of a bending device and the position of the exposed surface with regard to the magnetic stirrer at the bottom of beaker which modified the local stirring. This result suggested that, during the corrosion tests, a significant evolution of the chemical composition of the electrolyte should occur depending on the surface/solution volume ratio and on the solution stirring. To evaluate this effect, additional experiments were performed.

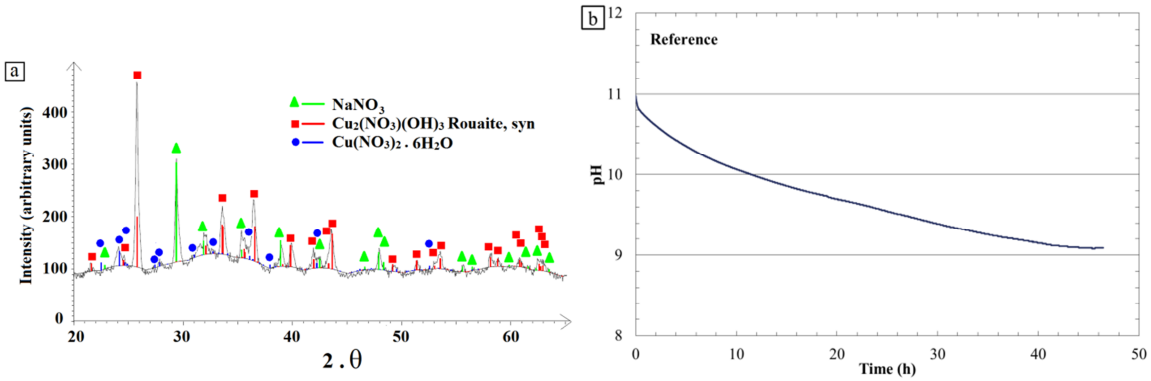

Figure 6. (a) XRD analysis of the blue corrosion products (b) pH vs. time during a corrosion test at the reference conditions, i.e., at 50 mV/SCE in a 0.5 M $NaNO_3$ solution at pH 11, performed on α,β' brass CuZn40Pb2.

Effect of chemical composition of the electrolyte versus time. The evolution of the corrosive solution during corrosion tests at a constant potential is expected to be a key factor on the dissolution kinetics, more precisely the solution in contact with the exposed surface, which can be different depending on the local stirring. In a first approach, the evolution of the bulk solution was studied. A blue coloring of the bulk due to the corrosion products was observed after a few hours of corrosion test. This evolution should correspond to a significant change in the aggressiveness of the environment that should modify the critical time corresponding to the transition from the first stage (similar kinetics for both dissolution processes) to the second stage (dezincification faster than

simultaneous dissolution). This finding meant that the critical time should be correlated with a critical chemical composition of the electrolyte.

Blue corrosion products in the solution were removed, dried and analyzed by XRD (Figure 6 a). $Cu_2(NO_3)(OH)_3$, called Rouaite, was identified and also $Cu(NO_3)_2$. The quantity of corrosion products accumulated on the surface that was exposed to the electrolyte and in the beaker seemed to be dependent on the pH of the solution, with more corrosion products at pH 12 compared to experiments at pH 11. Moreover pH vs. time data points that were measured for an experiment at the reference conditions (Figure 6 b) showed a decrease of the pH value over time, which was mainly related to the formation of the corrosion products. These results suggested a link between the evolution of the aggressiveness of the solution with the pH and the Cu concentration in solution.

To confirm the influence of the evolution of the chemical composition of the corrosive solution on the dissolution kinetics, dissolution kinetics were determined for two additional values of the ratio of the surface exposed to the electrolyte to the volume of the solution (S/V) generating different rates of corrosion product accumulation (Figure 7). Experiments were performed at a constant volume (300 mL in a beaker, without the bending device) with 0.02cm² and 4cm² of the surface exposed (respectively S/V=$6.7.10^{-5}$cm²/mL and $1.3.10^{-2}$cm²/mL) compared to the ratio used for previous experiments i.e., $6.7.10^{-4}$cm²/mL with 0.2cm² of surface exposed. The results clearly showed that an increase in the S/V value shifted the critical time to a lower value, i.e., led to a more rapid differentiation of the dezincification and simultaneous dissolution fronts (Figure 7 b). However, mainly for long tests (> 40h), the dezincification depths were smaller for the large S/V value while the simultaneous dissolution depths were quite similar whatever the ratio (Figure 7a).

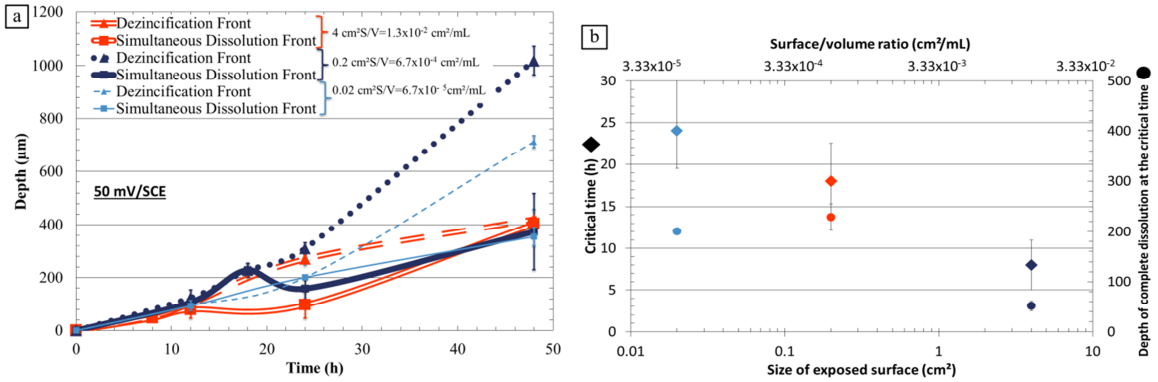

Figure 7. (a) Dissolution kinetics of the α,β' brass CuZn40Pb2 in a 0.5M $NaNO_3$ solution, pH 11 for different surface/volume ratios (b) critical time versus the surface/volume ratio. All of the measurements were performed for three values of the surface/volume ratio. The ratio $6.7.10^{-4}$ cm²/mL corresponded to a surface exposed to 0.2 cm^2, i.e., that of the previous experiments (Figure 4 a).

Discussion

Anodic dissolution of the β' phase was observed during corrosion tests in the reference solution (a 0.5 M $NaNO_3$ solution, pH 11) at a constant potential of 50 mV/SCE. The first

stage corresponded with a simultaneous dissolution of the β' phase, essentially the Zn and Cu content, through the following possible reactions [1-6].

$Zn_{(s)} + 2HO^- \rightarrow Zn(OH)_{2\,(s)} + 2e^-$ (precipitation white color) [1]
$Zn_{(s)} + 3HO^- \rightarrow HZnO_2^- + H_2O + 2e^-$ (at pH 11) [2]
$Zn_{(s)} + 4HO^- \rightarrow ZnO_2^{2-} + 2H_2O + 2e^-$ (at pH 11) [3]
$Cu_{(s)} + 2HO^- \rightarrow Cu(OH)_{2\,(s)} + 2e^-$ (precipitation blue color) [4]
$Cu_{(s)} + 3HO^- \rightarrow HCuO_2^- + H_2O + 2e^-$ [5]
$Cu_{(s)} + 4HO^- \rightarrow CuO_2^{2-} + 2H_2O + 2e^-$ [6]

During the second stage, the dissolution rate of Zn was faster than that of Cu [1-3] [4-6] in the β' phase. The values of the solution pH, the applied potential, the nature of the mechanical stress were identified in significantly influencing the kinetics of the two dissolution processes of the β' phase, i.e., simultaneous dissolution and dezincification, throughout the material. In the following part, their influence on the dissolution kinetics will be discussed, beginning with the initiation step and then followed by the propagation step. The initiation step was considered as the period before the dissolution goes in depth and the propagation step was the period where the dissolution was quantified by the OM observations in the cross-sections. Therefore, the initiation step corresponds to the period during which the dissolution was contained to the extreme surface. When the dissolution starts to be quantifiable with depth measurements by OM in cross section, it corresponds to the beginning of the propagation step.

Initiation step

Influence of pH. The nature of the Cu and Zn corrosion products that were observed depended upon the pH according to the different potential-pH diagrams; depending on the corrosion products present on the surface sample, it was assumed that the kinetics of dissolution could be affected. Taking into account this data, the low dissolution kinetics observed at pH 12 during the first hours can be explained. At this stage for a pH of 12, a larger amount of the blue corrosion products was observed in the solution compared to pH 11. The corrosion products were predominantly identified as Rouaite. They seemed to be sufficiently adhesive on the material to generate the pseudo-passivity stage and to slow down the dissolution processes during a relatively short time period (12 h at pH 12). Figure 6 b is in agreement with the expected reaction [1-6]. It was assumed that, when a sufficient drop in the pH value was achieved at the surface, a part of the hydroxide (Rouaite) that was formed dissolved and the pseudo-passivity stage was over, leading to an increase of the dissolution kinetics.

Influence of potential. It was also shown that, for a low potential, i.e., 20 mV/SCE, the dissolution kinetics were very low in the first stage defined on the dissolution kinetics versus time curves (Figure 4 a). This could be expressed as the existence of an incubation time; after this incubation time, a polarization of the brass at 20 mV/SCE led to an active dissolution process. This could be explained by a time necessary to achieve the breakdown of the material passivity. As shown by Fernandez et al. (21), when an intensity-potential curve is plotted, a higher scan rate moves the breakdown potential to more anodic values and vice versa. Further experiments should be performed to determine if a pseudo breakdown potential - much lower - exists as identified by

Fernandez *et al.* (21) for α-brass. Under this pseudo breakdown potential, the dissolution processes could not be propagated in depth.

Influence of a mechanical stress. This parameter did not show a significant impact on the initial stage of the dissolution process.

Propagation step

Parameters identified as relevant in explaining the dissolution kinetics during the propagation step are discussed below: the chemical composition of the solution was expected to be the key parameter.

Influence of pH. The active dissolution of the α,β'-brass, with a rate increasing with the depth of dissolution as observed in Figure 4 should be explained by the global decrease of the pH during the corrosion test (Figure 6 b). Indeed, a decrease in the pH could increasingly reduce the precipitation of the copper hydroxide, which should limit dissolution and also facilitate a mechanism of local acidification as proposed by Fernandez et al. (21).

Influence of corrosion product concentration. During the corrosion test, corrosion products accumulation is not negligible according to the precipitation observed and characterized by XRD (Figure 6 a). In particular, the Cu concentration increase was expected to control at least partially the dissolution kinetics. Indeed, previous studies in the literature (26) demonstrated the major role of the copper concentration in solution on the transition between the simultaneous and preferential (dezincification) dissolution of the Cu/Zn elements.

The first hypothesis states that copper in solution accelerates the dezincification process through a reaction [7]. This corresponds to a two stages-dezincification process: a simultaneous Cu/Zn dissolution followed by a second stage with Cu re-deposition from solution.

$$2Cu^{+} + Zn_{(s)} \rightarrow 2Cu_{(s)} + Zn^{2+} \qquad [7]$$

However, this re-deposition corresponds to the reduction of copper on the sample surface. Under anodic polarization, this reaction is quite unlikely, as postulated by Pchelnikov *et al.* (16). Moreover, the analysis of the Cu-rich phase due to the β' dezincification showed a Sn content and distribution similar to that of the non-corroded β' phase (Figure 3 b). Therefore, it seems irrelevant to assume that the β' phase was totally dissolved. This mechanism, including a total dissolution of the β' phase, can be excluded.

The other hypothesis corresponds to a second dezincification mechanism controlled by Zn diffusion. This hypothesis is compatible with the chemical composition of the Cu-rich phase, and, in particular, with its Sn content. In this mechanism, Zn is preferentially dissolved; dezincification goes on through the material due to Zn diffusion through the porous Cu-rich phase that has been formed. However, no gradient of Zn was observed throughout the Cu-rich phase (Figure 3 b), which is usually observed in the case of Zn diffusion-controlled mechanisms. This observation might put in doubt this hypothesis.

On balance, the two mechanisms proposed do not fit perfectly with the usual observations found in literature. However, the Cu concentration in solution should be considered as a relevant parameter, for example as a solubility limit achievement for Cu, which should explain the transition between the simultaneous dissolution process and the dezincification process. This transition was identified for each of the experiments performed using a different S/V ratio which corresponded with different Cu and Zn concentrations in the bulk. The relationship between the dissolution kinetics and the S/V ratio should be easily correlated to a corrosion product accumulation rate in particular Cu accumulation near the corroded surface. A critical Cu content in the bulk of 6-8 $mg.cm^{-2}.L^{-1}$ was determined. When this critical Cu concentration in solution was reached, the equilibrium between the two dissolution mechanisms was modified, leading to a faster Zn dissolution compared to the Cu dissolution and therefore promoting the Zn dezincification compared to the simultaneous dissolution. As a remainder, it is worth noticing that the Cu concentration at the bottom of the corrosion defects that were formed should be significantly different than that measured in the bulk; this concentration should be the one to consider, And so, it should be assumed that the deeper the corrosion defects, the shorter the time necessary to reach the critical Cu concentration. However, in first approach, taking into account the concentration in the bulk seemed to be relevant.

Concerning the Zn dezincification process throughout the material, no gradient of Zn through the Cu-rich phase that was formed was noticed. Regarding the high Zn proportion in the β' phase, the defect density of the β' phase should be considered as strong after dezincification, and much more than for the α phase of α-brass. According to the literature, it was demonstrated that dezincification induced a tensile stress in the dezincification layer of brass (23) (27) (28). The assumption here is that, for the β'-phase in α-β' brass, the stress level could be high enough to induce the coalescence of the defects and then create porosity, more specifically, open porosity. OM observations were in agreement with this statement. For α-brass with the Zn content being lower, this phenomenon could not occur. This should explain the changes in the mechanism of dezincification between the α-β' brass and the α-brass. A rapid dissolution of Zn through the pores of the Cu-rich phase, i.e., through the liquid phase trapped inside the pores and not through the solid Cu-rich phase, could explain this phenomenon. Assuming the above, the Cu concentration had to be considered as a key parameter in both dissolution processes. It had been previously noticed that the evolution of the chemical composition of the solution could be largely affected by local stirring (see for example the problems of the accumulation of the corrosion products from the sample surface when the bending device was used). In the framework of the development of an accelerated SCC test, the geometry of the experimental device correlated to a local stirring that was identified as one of the key parameters.

Influence of a mechanical stress. A significant effect of the mechanical stress on the dissolution kinetics (free of bending device effect) was demonstrated (Figure 5). On the one hand, a compressive mechanical stress promoted the simultaneous dissolution to the detriment of dezincification. When a favorable environment was achieved to promote dezincification, the porosity of the Cu-rich phase that was formed was closed by the effects of the compressive mechanical stress. If the dezincification mechanism was controlled by the diffusion of Zn^{2+} in the liquid phase, the decrease in the dezincification is in agreement with the results. On the other hand, a mechanical tensile stress accelerated the dezincification process. When the critical Cu-value was reached that promoted the

dezincification kinetics, the porosity of the Cu-rich phase that was formed was opened due to the tensile stress. Therefore, if the dezincification mechanism was controlled by the diffusion of Zn^{2+} in liquid phase, the dezincification process would be accelerated, as was observed.

Conclusions

Results presented in this study, concerning the α,β'-brass CuZn40Pb2 in $NaNO_3$ solutions are summarized below.

- The typical corrosion damage observed after corrosion tests, in a 0.5 M $NaNO_3$ solution at pH 11 at a constant anodic potential of 50mV/SCE, was the dissolution of the β' phase.
- For a lower potential (20mV/SCE), an incubation time, before dissolution occurred through the material, was observed.
- At higher pH (13), a pseudo-passivity stage could be achieved because of the accumulation of hydroxide copper.
- The dissolution process through the material was described with two propagation stages: an initial stage corresponding to the simultaneous dissolution of copper and zinc, followed by a second stage called dezincification where the Zn dissolution was faster than that of copper.
- The process of dezincification proposed was based on Zn diffusion through the pores of the Cu-rich phase that was formed. These pores were assumed to be due to the β' phase dezincification and the stress induced.
- The porosity of the Cu-rich phase was significantly affected by an external mechanical stress which consequently affected the kinetics of the β' phase dezincification and/or its simultaneous dissolution.
- The bending device built for the experiments allowed to study the dissolution kinetics of the α,β'-brass. The conditions of the accelerated tests allowed to obtain relevant results.

This work was performed in the framework of the CETIMAT. The CIRIMAT and the CETIM collaborate for certain aspects of their research activities; this collaboration is performed in a joint laboratory, called CETIMAT.

Acknowledgments

The authors would like to express their sincere thanks to J-C. Salabura for the design of the bending device utilized in the study and R.Mainguy for providing the technical support to establish the experimental device.

References

1. J. Yu and R. N. Parkins, *Corros. Sci.*, **27**(2), 159 (1987).
2. J. Yu, R. N. Parkins, Y. Xu, G. Thompson and G. C. Wood, *Corros. Sci.*, **27**(2), 141 (1987).

3. R. B. Rebak, R. M. Carranza and J. R. Galvele, *Corros. Sci.*, **28**(11), 1089 (1988).
4. A. T. Cole, R. C. Newman and K. Sieradzki, *Corros. Sci.*, **28**(1), 109 (1988).
5. R. M. Carranza and J. R. Galvele, *Corros. Sci.*, **28**(9), 851 (1988).
6. D. Wu, H. S. Ahluwalia, H. Cai, J. T. Evans and R. N. Parkins, *Corros. Sci.*, **32**(7), 769 (1991).
7. F. Mackay, J. T. Evans and R. N. Parkins, *Corros. Sci.*, **33**(5), 699 (1992).
8. E. A. Ashour and B. G. Ateya, *Corros. Sci.*, **37**(3), 371 (1995).
9. M. G. Alvarez, P. Lapitz, S. A. Fernandez and J. R. Galvele, *Corros. Sci.*, **47**, 1643 (2005).
10. P. Lapitz, J. Ruzzante and M. G. Alvarez, *Corros. Sci.*, (49), 3812 (2007).
11. M. B. Hintz, L. J. Nettleton and L. A. Heldt, *Metall. Trans. A*, **16A**, 971 (1985).
12. M. B. Hintz, W. K. Blanchard, P. K. Brindley and L. A. Heldt, *Metall. Trans. A*, **17A**, 1081 (1986).
13. F. Zucchi, G. Trabanelli, M. Fonsati and A. Giusti, *Mater Corros*, **49**, 864 (1998).
14. B. Assouli, A. Srhiri and H. Idrissi, *NDT&E Int.*, **36**, 117 (2003).
15. L. Burzynska, *Corros. Sci.*, **43**, 1053 (2001).
16. A. P. Pchelnikov, A. D. Sitnikov, A. K. Marshakov and V. V. Losev, *Electrochim. Acta*, **26**(5), 591 (1981).
17. E. Brandl, R. Malke, T. Beck, A. Wanner and T. Hack, *Mat. Corros.*, **60**(4) (2009).
18. E. Sarver and M. Edwards, *Corros. Sci.*, **53**, 1913 (2011).
19. C. Mapelli, A. Gruttadauria and M. Bellogini, *Eng. Fail. Anal.*, **17**, 431 (2010).
20. C. Mapelli, D. Mombelli, S. Barella and A. Gruttadauria, *Eng. Fail. Anal.*, **27**, 141 (2013).
21. S. A. Fernandez and M. G. Alvarez, *Corros. Sci.*, **53**, 82 (2011).
22. T. KG. Namboodhiri, R. S. Chaudhary, B. Prakash and M. K. Agrawal, *Corros. Sci.*, **22**(11), 1037 (1982).
23. J. J. Podesta, G. P. Rothwell and T. P. Hoar, *Corros. Sci.*, **11**, 241 (1971).
24. T. J. Kagetsu and W. F. Graydon, *J. Electrochem. Soc.*, **110**(7), 709 (1963).
25. J. Bumbulis and W. F. Graydon, *J. Electrochem. Soc.*, **109**(12), 1130 (1962).
26. A. V. Polunin, A. P. Pchelnikov, V. V. Losev and I. K. Marshakov, *Electrochim. Acta*, **27**(4), 467 (1982).
27. H. Lu, K. Gao and W. Chu, *Corros. sci.*, **40**(10), 1663 (1998).
28. X. J. Guo, K. W. Gao, L. J. Qiao and W. Y. Chu, *Corros. Sci.*, **44**, 2367 (2002).